AGU PUBLICATIONS

JGR

Journal of Geophysical Research: Oceans

RESEARCH ARTICLE

10.1002/2015JC011329

# Upper-ocean mixing due to surface gravity waves

**Lichuan Wu[1], Anna Rutgersson[1], and Erik Sahlée[1]**

[1]Department of Earth Sciences, Uppsala University, Uppsala, Sweden

**Key Points:**
- Nonbreaking waves and Langmuir turbulence are the most important terms from waves on ocean mixing
- 2-D wave spectrum should be used to calculate the wave induced ocean mixing if possible
- Under high-wave conditions, nonbreaking-wave-induced mixing cannot be ignored

**Correspondence to:**
L. Wu,
wulichuan0704@gmail.com

**Citation:**
Wu, L., A. Rutgersson, and E. Sahlée (2015), Upper-ocean mixing due to surface gravity waves, *J. Geophys. Res. Oceans*, *120*, doi:10.1002/2015JC011329.

Received 21 SEP 2015
Accepted 30 NOV 2015
Accepted article online 8 DEC 2015



**Abstract** Surface gravity waves play an important role in the lower layer of the atmosphere and the upper layer of the ocean. Surface waves effect upper-ocean mixing mainly through four processes: wave breaking, Stokes drift interaction with the Coriolis force, Langmuir circulation, and stirring by nonbreaking waves. We introduce the impact of these four processes into a 1-D $k-\epsilon$ ocean turbulence model. The parameterizations used are based mainly on existing investigations. Comparison of simulation results and measurements demonstrates that considering all the effects of waves, rather than just one effect, significantly improves model performance. The nonbreaking-wave-induced mixing and Langmuir turbulence are the most important terms when considering the impact of waves on upper-ocean mixing. Under high-wave conditions, the turbulent mixing induced by nonbreaking waves can be of the same order of magnitude as the viscosity induced by other terms at the surface. Nonbreaking waves contribute very little to shear production and their impact is negligible in the models. Sensitivity experiments demonstrate that the vertical profile of the Stokes drift calculated from the 2-D wave spectrum improves model performance significantly compared with other methods of introducing wave effects.

## 1. Introduction

The ocean surface, which covers to 70% of the global surface area, is generally covered by surface gravity waves, which are very important for the ocean circulation and air-sea fluxes. It is estimated that the global wind energy input to the geostrophic current is 0.9 TW and to the Ekman layer is 3 TW; however, 60 TW is transported from the wind to surface waves [*Qiao and Huang*, 2012]. In ocean general circulation models (OGCMs), the impact of surface waves is not usually directly considered, though it is sometimes partly considered. OGCMs reportedly underestimate the mixed layer depth (MLD) and overestimate the sea surface temperature (SST) in some areas [e.g., *Qiao et al*., 2004]. Some studies [i.e., *Qiao et al*., 2004; *Hu and Wang*, 2010; *Qiao et al*., 2013] arrive at improved simulation results when the impact of surface waves on ocean mixing is taken into account. Surface waves affect upper-ocean mixing mainly through four processes: (1) wave breaking, (2) the Coriolis-Stokes force (CSF), (3) Langmuir circulation, and (4) nonbreaking-wave-induced mixing.

Measurements and numerical simulations indicate that wave breaking causes significant loss of both momentum and energy fluxes from waves [e.g., *Melville et al*., 2002]. Wind energy generates turbulence in the upper-ocean layer, mainly to a depth of a few significant wave heights from the surface [i.e., *Terray et al*., 1996; *D'Asaro*, 2014]. Large-eddy simulation and direct numerical simulation, also used to study the impact of wave breaking on ocean mixing [i.e., *Noh et al*., 2004; *Sullivan et al*., 2004, 2007], indicate that breaking waves can affect the ocean surface layer.

The effect of the Stokes drift (i.e., the mean temporal and spatial difference between the Eulerian and Lagrangian velocities, $\mathbf{u_s}$) on the ocean mean flow is exerted through two processes. One is the interaction with the Coriolis effect, which yields the term CSF, i.e., $\mathbf{f_c}\times\mathbf{u_s}$, for the momentum equations, where $\mathbf{f_c}$ is the Coriolis parameter. The other process is Langmuir circulation (LC) through the action of a Stokes-vortex force, i.e., $\mathbf{u_s}\times\boldsymbol{\omega_v}$, where $\boldsymbol{\omega_v}$ is the vortex vector. Numerical and theoretical analyses demonstrate that the CSF is an important mechanism controlling upper-ocean dynamics [i.e., *Polton et al*., 2005; *Wu and Liu*, 2008; *Deng et al*., 2012, 2013]. *Wu and Liu* [2008] demonstrated that the Stokes drift not only changes the wind energy input to the Ekman layer but also redistributes the total energy input between the direct wind energy input and the Stokes drift-induced energy input. The turbulent Langmuir number, $La=\sqrt{u_{w*}/U_{s0}}$, is an index of the significant contribution of LC to ocean mixing, where $u_{w*}$ is the frictional velocity in water and $U_{s0}$ the surface Stokes drift velocity [e.g., *McWilliams et al*., 1997]. Langmuir turbulence is transformed

into shear turbulence during the $La \sim 0.5$–2 regime [i.e., *Li et al*., 2005; *Grant and Belcher*, 2009; *Belcher et al*., 2012; *Sutherland et al*., 2013]. It is generally accepted that LC can influence ocean mixing, so how to parameterize its impact in OGCMs is an important issue.

Nonbreaking-wave-induced ocean mixing is a direct stirring function of waves. Numerical simulations, theoretical analyses, and laboratory experiments have demonstrated that nonbreaking waves can generate turbulence [i.e., *Qiao et al*., 2004; *Babanin*, 2006; *Dai et al*., 2010; *Pleskachevsky et al*., 2011; *Babanin and Chalikov*, 2012; *Savelyev et al*., 2012; *Tsai et al*., 2015] and that their intensity is related to the wave state [i.e., *Qiao et al*., 2004; *Babanin*, 2006; *Pleskachevsky et al*., 2011]. From the turbulent kinetic energy (TKE) dissipation rate induced by wave turbulence interaction, some parameterizations have been proposed and applied to improve the performance of OGCMs and coupled models [i.e., *Huang and Qiao*, 2010; *Ghantous and Babanin*, 2014; *Li et al*., 2014; *Fan and Griffies*, 2014]. As expected, parameterizations of nonbreaking-wave-induced mixing improve the performance of models when they are applied to OGCMs [i.e., *Qiao et al*., 2010; *Hu and Wang*, 2010; *Huang et al*., 2011]. However, as argued by *Kantha et al*. [2014], some parameterizations overestimate the wave contribution to ocean mixing, possibly because they do not clearly distinguish the part of the turbulence contributed by LC from that contributed by nonbreaking waves (wave stirring).

In the study of *Kantha and Clayson* [2004], the TKE injected from breaking waves and LC were added into Mellor-Yamada (MY) turbulence closure scheme [*Mellor and Yamada*, 1982] as the surface boundary condition. The influence of LC was added into the total shear production in the two turbulence equations [*Kantha and Clayson*, 2004]. Ideal simulations and realistic simulations at OWS Papa station indicate that the effect of breaking waves on the mixed layer are small compared with the effect from LC. Instead of relating the surface TKE flux (breaking wave induced energy flux) to the wind stress [*Craig and Banner*, 1994; *Kantha and Clayson*, 2004], the TKE injection was calculated by the use of wave-energy dissipation spectrum in the study of *Paskyabi et al*. [2012]. A wave-induced transfer of momentum term was added to the momentum equations. Compared with the effects of breaking waves, simulation results indicate that the effect of CSF (which is added into the momentum equations) is relative larger [*Paskyabi et al*., 2012]. In the recent study [*Paskyabi and Fer*, 2014], the wave influences investigated in *Paskyabi et al*. [2012] and the shear production by LC were added to a $k-\epsilon$ turbulence scheme in a 1-D ocean model. The simulation results were compared with the measured dissipation rate, which show that the breaking wave influence is mainly on the surface layer. Adding the Stokes production (CSF and shear production from LC) improves the agreement more than breaking waves [*Paskyabi and Fer*, 2014]. In the study of *Janssen* [2012], the wave influences were applied to a 1-D turbulence model to the Arabian Sea data [*Weller et al*., 2002]. The simulations show that the breaking wave influence dominates the wave influence on the very surface layer, the influence of the Stokes drift can improve the model performance during the deeper layer [*Janssen*, 2012]. Compared with breaking wave induced mixing, the effect of which is mainly on a few significant wave heights depth, the nonbreaking-wave-induced mixing can effect much deep layer [*Qiao et al*., 2004, 2010]. In the study of *Qiao and Huang* [2012], they compared the influence of vertical shear mixing and nonbreaking-wave-induced mixing in the extratropical ocean from ocean model simulations. The results indicate that nonbreaking-wave-induced mixing is more important than the influence of vertical shear mixing [*Qiao and Huang*, 2012].

In this study, based on the results of various investigations, we aim to distinguish the contributions of various waves, i.e., breaking waves, CSF, LC and nonbreaking waves, and to prevent them from being repeatedly considered in parameterizations of wave impact on ocean mixing. We also aim to consider all wave-induced processes both separately and in combination within the same study to evaluate their relative importance. The wave contributions to upper-ocean mixing are applied to the $k-\epsilon$ turbulence equations, which are used in a 1-D ocean model to investigate their impacts. This paper is organized as follows: section 2 describes the theory of wave impact on the upper ocean; section 3 describes the model used in this study, the experimental design, and the data used in the simulations; the simulation results are presented in section 4; the results are discussed in section 5 and conclusions are summarized in section 6.

## 2. Theory

### 2.1. Breaking Wave Impact on the Ocean Mixing

Breaking waves cause significant momentum and energy fluxes losses from waves. The lost momentum flux is transferred to the underlying currents, while the lost energy flux is transferred mainly to near-surface

turbulence [*He and Chen*, 2011]. The momentum and energy flux losses from waves are related to the wave-breaking probability, which is in turn related to the wind speed. *He and Chen* [2011] demonstrated that the impact on ocean mixing of the momentum induced by breaking waves is larger than that of the energy fluxes induced by breaking waves.

Considering the breaking-wave-induced energy in the upper-ocean turbulence, *Craig and Banner* [1994] proposed a model including the effect of wave breaking, in which wave breaking is treated as an additional input into the TKE at the surface boundary, as follows [*Craig and Banner*, 1994]:

$$q_{wb,0}=m_0\rho_w u_{w*}^3 \tag{1}$$

where $m_0$ is a coefficient, treated as 100 in this study, following *Craig and Banner* [1994], and $\rho_w$ the sea water density.

Based on the studies of *Sullivan et al*. [2004, 2007] and *He and Chen* [2011] estimated the breaking-wave-induced stress, $\tau_{wb}(z)=\langle A\rangle(z)\triangle z$, transferred from surface wave breaking to ocean currents, expressed as [*He and Chen*, 2011]:

$$\int_{-H}^{z}\langle A\rangle(z)dz/\left\{\gamma\rho_a u_*^2\right\}\approx e^{bz} \tag{2}$$

where $b$ is a coefficient depending on the wind speed, $\langle A\rangle$ the momentum density, $u_*$ the atmospheric friction velocity, $\rho_a$ the air density, $H$ the water depth, and $\gamma$ the ratio of the breaking stress to the wind stress. As mentioned by *He and Chen* [2011], $\gamma$ should be related to the wave condition or wind condition, though its function of $\gamma$ is still unclear. *He and Chen* [2011] treated $\gamma$ as constant at 0.2 when they simulated data from the Papa ocean weather station; here, we also treat it as constant at 0.2 when simulating data regarding conditions at the Papa station. For the coefficient $b$, we interpolated it to different wind speeds following the results of *He and Chen* [2011].

In this study, taking account of the impact of breaking waves means takes account both breaking-wave-induced energy in the surface boundary (equation (1)) and breaking-wave-induced stress on the mean flow (equation (2)).

### 2.2. Stokes Drift Impacts on the Ocean Mixing

The CSF and the LC both result from the interaction of the Stokes drift with other terms. When the 2-D wave spectrum is available, the Stokes drift can be calculated as:

$$\mathbf{u_s}=\frac{16\pi^3}{g}\int_0^{\infty}\int_{-\pi}^{\pi}f^3S_{f\theta}(f,\theta)\exp\left(\frac{8\pi^2f^2z}{g}\right)d\theta df \tag{3}$$

where $f$ is the wave frequency, $\theta$ the wave direction, and $S_{f\theta}$ the directional frequency spectrum.

The CSF can be understood as originating in the fact that "the Stokes drift attempts to tilt and stretch the planetary vorticity into the horizontal leading to a vortex force on the flow" [*Polton et al*., 2005]. The CSF exerts a noticeable influence on the ocean circulation in terms of the mixed-layer temperature and MLD [*Deng et al*., 2013]. The CSF is usually considered in OGCMs by adding an extra term (i.e., $\mathbf{f_c}\times\mathbf{u_s}$) to the momentum equations.

Since LC has been observed [*Langmuir et al*., 1938], much effort has focused on the mechanisms of LC and the extent of its effect on ocean mixing in the upper-ocean layer [i.e., *Craik and Leibovich*, 1976; *Li et al*., 1995; *McWilliams and Sullivan*, 2000]. Incorporating the impact of LC into OGCMs has been investigated in several studies. *Axell* [2002] introduced LC production as an extra shear production term in the $k-\epsilon$ turbulence model, which was applied in the Nucleus for European Modelling of the Ocean (NEMO) model [*Madec*, 2008]. To consider the effect of LC, *McWilliams and Sullivan* [2000] modified the turbulence velocity scale in the K-profile ocean boundary layer parameterization (KPP) scheme by multiplying it by a Langmuir turbulence enhancement factor. Later, *Smyth et al*. [2002] introduced the stratification effect into the parameterization of *McWilliams and Sullivan* [2000]. Some studies treat LC as only the Stokes drift shear production, adding this Stokes drift shear production to the total shear production in the TKE [i.e., *Ardhuin and Jenkins*, 2006; *Li et al*., 2013a]. In addition to the Stokes drift shear production, in the study of *Kantha and Clayson* [2004], an extra boundary energy term contributed from LC was added to the boundary condition in MY

turbulence scheme [*Mellor and Yamada*, 1982] and some adjustment about the coefficients in MY scheme was done. To avoid repeatedly considering other wave impact terms, in this study, we added the LC-generated shear production to the TKE to consider its impact on the ocean vertical mixing, as follows:

$$P_{LC}=\nu_t\left[\frac{\partial u}{\partial z}\frac{\partial u_s}{\partial z}+\frac{\partial v}{\partial z}\frac{\partial v_s}{\partial z}\right] \tag{4}$$

where $\nu_t$ is the eddy viscosity and $u$ and $v$ are the velocities in the eastward and northward directions, respectively. The Stokes drift velocities in the eastward and northward directions are denoted $u_s$ and $v_s$, respectively.

### 2.3. Nonbreaking Wave Impact on the Ocean Mixing

How to incorporate the effect of nonbreaking waves on ocean mixing into OGCMs is an open scientific question. In view of wave-induced Reynolds stress, some studies have proposed nonbreaking-wave-induced mixing parameters, which have been added to the turbulent viscosity in models [i.e., *Qiao et al*., 2004; *Hu and Wang*, 2010; *Pleskachevsky et al*., 2011], producing some improvements in the simulation results. *Pleskachevsky et al*. [2011] parameterized the impact of nonbreaking waves on ocean mixing by modifying the turbulent viscosity and adding the shear production induced by nonbreaking waves.

*Pleskachevsky et al*. [2011] divided the contribution of wave motion to ocean mixing into two parts: (1) symmetric wave motion subprocesses, which do not contribute to mean currents but do affect the turbulence, and (2) asymmetric wave motion mean-flow processes, which contribute to mean currents. Based on linear wave theory, the wave contribution to these subprocesses is expressed as the nonbreaking-wave-induced mixing, expressed as [*Pleskachevsky et al*., 2011]:

$$\nu_{wave}=l_{wave}^2 M_{wave}^{SM} \tag{5}$$

where $l_{wave}$ is the length scale of the wave-induced turbulence, $M_{wave}^{SM}$ is the contribution of symmetric wave motion to shear, $M_{wave}^{SM}=\bar{M}_{wave}$, and $\overline{M_{wave}{}^2}$ is the mean value of the shear frequency of the wave motion.

The contribution of asymmetric-wave-motion shear to the mean flow can be expressed by *Pleskachevsky et al*. [2011]:

$$M_{wave}^{AM}=k_{wave}^{AM}M_{wave}^{SM} \tag{6}$$

where $k_{wave}^{AM}$ is the relationship between wave-energy dissipation and total wave energy. Following *Pleskachevsky et al*. [2011], we treat $k_{wave}^{AM}$ as constant at $1.5\times10^{-4}$. The condition of nonbreaking waves generating turbulence is indicated by the Reynolds number, $Re^{wave}(z)$, being larger than the critical Reynolds number, $Re_{crit}^{wave}$. Following *Babanin* [2006] and *Pleskachevsky et al*. [2011], the critical Reynolds number is set to 3000.

The wave-induced shear production is then:

$$P_{wave}=\nu_t(M_{wave}^{AM})^2 \tag{7}$$

## 3. Model and Experiments

### 3.1. GOTM

The General Ocean Turbulence Model (GOTM) is a 1-D water column model of the thermodynamic and hydrodynamic processes related to vertical mixing in water [*Umlauf and Burchard*, 2005]. GOTM has been widely used to study the problems of ocean mixing [*He and Chen*, 2011; *Li et al*., 2013b; *Drivdal et al*., 2014; *Ghantous and Babanin*, 2014]. The momentum equations in GOTM are expressed as follows:

$$\partial_t u=\underbrace{\partial_z((\nu_t+\nu)\partial_z u)}_{a}\underbrace{-g\partial_x\zeta}_{b}\underbrace{+f_c v}_{c}\underbrace{+f_c v_s}_{d}\underbrace{+\tau_{wb,x}}_{e} \tag{8}$$

$$\partial_t v=\underbrace{\partial_z((\nu_t+\nu)\partial_z v)}_{a}\underbrace{-g\partial_y\zeta}_{b}\underbrace{-f_c u}_{c}\underbrace{-f_c u_s}_{d}\underbrace{+\tau_{wb,y}}_{e} \tag{9}$$

where $x$, $y$, and $z$ are eastward, northward, and upward directions, respectively, $t$ is time, $\zeta$ surface elevation, $\nu$ molecular diffusivity, and $g$ gravitational acceleration. Term ($a$) is the sum of the turbulence and viscous

transport terms, (*b*) the pressure gradient, (*c*) the Coriolis force, (*d*) the CSF, and (*e*) the breaking-wave-induced stress. The direction of $\tau_{wb}$ is aligned with the wind direction; $\tau_{wb,x}$ and $\tau_{wb,y}$ are the components of $\tau_{wb}$ in *x* and *y* directions, respectively.

In this study, the impact of waves on ocean mixing is introduced into a $k-\epsilon$ two-equation closure model to investigate the impact. The transport equation for the TKE, $k=q^2/2$, is:

$$\frac{\partial k}{\partial t}=\frac{\partial}{\partial z}\left(\frac{\nu_t}{\sigma_k}\frac{\partial k}{\partial z}\right)+P_s+P_b-\epsilon \tag{10}$$

where $\sigma_k$ is the constant Schmidt number, $P_s$ shear production, $P_b$ buoyancy production, and $\epsilon$ dissipation. The transport equation for dissipation is:

$$\frac{\partial \epsilon}{\partial t}=\frac{\partial}{\partial z}\left(\frac{\nu_t}{\sigma_\epsilon}\frac{\partial \epsilon}{\partial z}\right)+\frac{\epsilon}{q}\left[c_{\epsilon 1}P_s+c_{\epsilon 3}P_b-c_{\epsilon 2}\epsilon\right] \tag{11}$$

where $\sigma_\epsilon$ is the Schmidt number for $\epsilon$, and $c_{\epsilon 1}$, $c_{\epsilon 2}$, and $c_{\epsilon 3}$ are empirical coefficients. Shear production, $P_s$, is calculated by:

$$P_s=\nu_t\left[\left(\frac{\partial u}{\partial z}\right)^2+\left(\frac{\partial v}{\partial z}\right)^2\right] \tag{12}$$

The viscosity is calculated as:

$$\nu_t=c_\mu k^{1/2} l \tag{13}$$

where $c_\mu$ is the stability function and *l* a typical length scale. Considering the terms influenced by waves, total shear production, viscosity, and heat diffusion can be expressed as follows:

$$P_s'=P_s+P_{wave}+P_{LC} \tag{14}$$

$$\nu_t'=\nu_t+\nu_{wave} \tag{15}$$

$$\nu_h'=\nu_h+\nu_{wave} \tag{16}$$

where $\nu_h$ the heat diffusion.

### 3.2. Experimental Design

The Papa ocean weather station is located in the eastern subarctic Pacific (50°N, 145°W) in 4230 m deep water where the horizontal advection of heat and salt is assumed to be small [i.e., *Mellor and Blumberg*, 2004; *Li et al*., 2013b]. The data from the station are ideal for testing a 1-D model. Various authors have used data from this station for validating turbulence closure schemes [e.g., *Li et al*., 2013b]. In the present study, the simulation of data from the Papa station is used to investigate the effect of waves on ocean mixing. The water depth in the model is set to 250 m, deep enough to prevent surface mixing from reaching the bottom [*Burchard et al*., 1999]. The initial temperature data were obtained from measurements. The other settings of the model are the same as in the "OWS papa" scenario downloaded from the GOTM website, except for the changes when considering the impact of waves explained in the different experiments.

To investigate the various wave impacts on ocean mixing both separately and in combination, six experiments were designed, the details of which are presented in Table 1. The first experiment (Exp-1), uses the default setting of GOTM with the $k-\epsilon$ turbulence model without including the impact of breaking waves ($m_0=0$). In Exp-1, wave impact is not incorporated into the model, making it the control experiment. In Exp-2 to Exp-5, each of the wave impacts (described in sections 2.1–2.3) is added separately. In Exp-2, the effect of breaking waves (i.e., both breaking-wave-induced stress and energy flux) is added to the model (equation (1) and $\tau_{wb}$ in equations (8) and (9)). The impact of the CSF is added to the control experiment in Exp-3. In Exp-4, the impact of LC is introduced (equation (4)). The Stokes drift profiles used in Exp-3 and Exp-4 is calculated through equation (3) using the 2-D wave spectrum from WAM simulation (section 3.3). In Exp-5, the impact of nonbreaking waves on ocean mixing is added to the model (equations (7), (15), and (16)). All the wave impacts on ocean mixing are combined in the model in Exp-6.

**Table 1.** Setup of the Six Experiments[a]

| Experiments | Breaking Waves | CSF | LC | Nonbreaking Waves |
|---|---|---|---|---|
| Exp-1 | No | No | No | No |
| Exp-2 | Yes | No | No | No |
| Exp-3 | No | Yes | No | No |
| Exp-4 | No | No | Yes | No |
| Exp-5 | No | No | No | Yes |
| Exp-6 | Yes | Yes | Yes | Yes |

[a]Exp-1 is the Reference Case, Exp-2 to Exp-5 are the four experiments in which wave processes are studied separately, and exp-6 includes all wave contributions.

### 3.3. Data Used for Experiments

At the Papa ocean weather station, meteorological measurements are made of wind speed, wind direction, air temperature, air pressure, and the sea temperature and salinity profiles. The method for using bulk formulas for the surface momentum and heat fluxes is discussed in detail by *Burchard et al.* [1999]. When using the momentum and heat flux results from *Burchard et al.* [1999], we choose the year 1962 to investigate the effect of waves on ocean mixing.

The WAM model [*WAMDI*, 1988] is used to simulate the wave state. The ERA-40 wind data [*Uppala et al.*, 2005] are used to force the WAM model. The domain of the WAM model is 10–65°N and 120–175°W. To simulate the wave parameters and 2-D wave spectrum, a relative high resolution of simulation is necessary. In this study, the resolution of the simulation is 0.1° and 25 wave frequencies are simulated, ranging from 0.04177 to 0.41145 Hz. The wave direction resolution in the model is 30°. The 2-D wave-spectrum data, significant wave height, peak wave period, and other wave information are obtained from the WAM model.

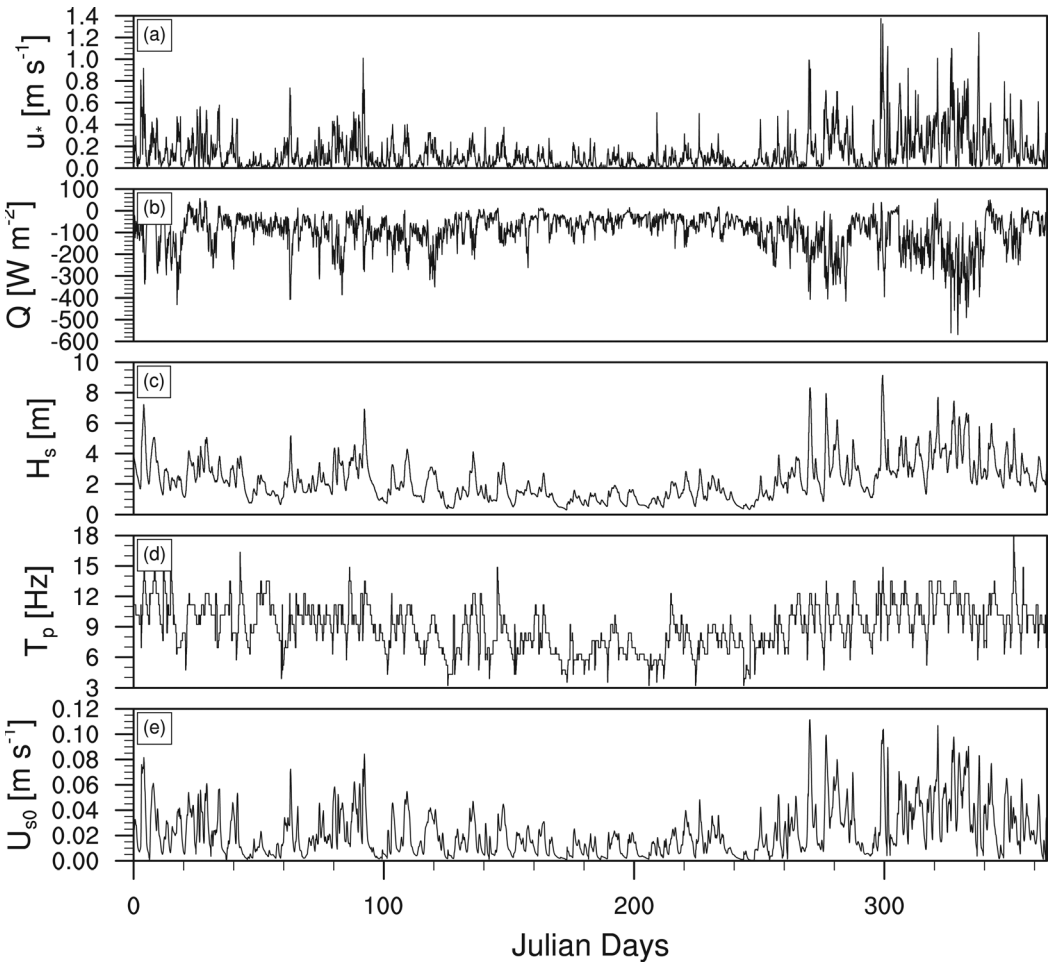


**Figure 1.** The forcing conditions of the 1-D model for 1962 at the Papa station. The forcing parameters are: (a) friction velocity, (b) surface heat flux, (c) significant wave height from the WAM model, (d) peak wave period, and (e) surface Stokes drift velocity from the WAM model.

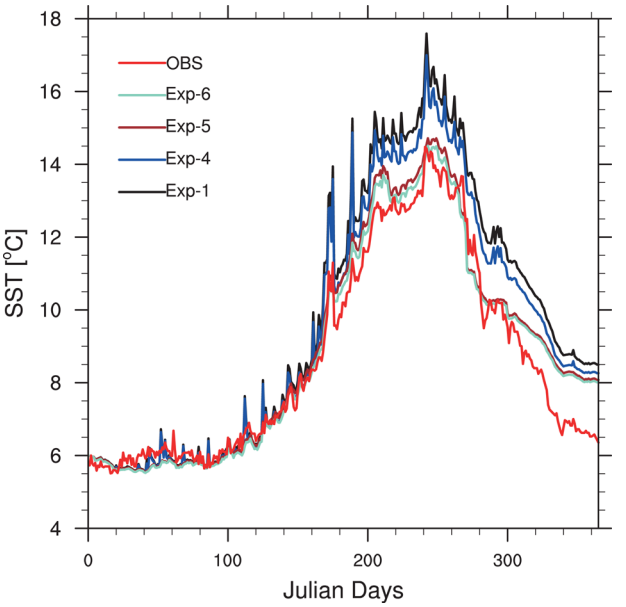


**Figure 2.** Simulated and observed SST from experiments and observations in 1962 (°C).

Figure 1 shows the forcing conditions in 1962. In the summer, the wind stress and significant wave height are small; in contrast, the maximum friction velocity exceeds 1 m $s^{-1}$ and the maximum significant wave height exceeds 7 m in winter. The maximum surface Stokes drift velocity in winter exceeds 0.2 m $s^{-1}$. The surface heat flux is negative most of the year (i.e., heat is transported from ocean to atmosphere). The peak wave frequency conditions in 1962 are shown in Figure 1d.

## 4. Results

### 4.1. Simulation Results

Figure 2 shows the SST simulated in all experiments except Exp-2 and Exp-3; as the simulation results of Exp-2 and Exp-3 differ little from those of Exp-1, they are not shown in the following figures. In summer, the control experiment (Exp-1, black line) gives SST results exceeding the measurements. Adding the impact of breaking waves (Exp-2) or the CSF (Exp-3) does not change the simulation results significantly. Adding the impact of LC (Exp-4) to the model, somewhat improves the results, giving a slightly lower SST. If the impact of nonbreaking waves (Exp-5) is added to the model, the SST in summer is several degrees lower and the model performs significantly better than in the other experiments. Adding all the wave impacts to the model (Exp-6) results in the best SST performance of all the experiments.

The time series of the vertical profiles of the temperature difference between the simulation results and the measurements are shown in Figure 3. From January to June, the simulation results of the six experiments agree well with the measurements in the upper layer (0–70 m), though, in the 70–120 m layer (which is around the MLD), the simulations underestimate the temperature by about 0.6°C. From July to December, simulations Exp-1 to Exp-4, which exclude the impact of nonbreaking waves, overestimate the temperature in the upper layer; when this impact is included, as in Exp-5 and Exp-6, the model slightly overestimates the temperature in the MLD.

The MLD is defined as the depth at which the temperature is 0.2°C lower than the SST. Table 2 shows the statistical results for the MLD. Considering all the wave impacts increases the ocean mixing, in turn reducing the mean error (ME, i.e., simulation minus observation) and mean absolute error (MAE) of the MLD of the upper-layer temperature (0–20 m). The mean temperature differences at various depths are shown in Figure 4 and the statistical results for temperature in the 0–20 m layer in Table 2. Introducing breaking waves (Exp-2) and the CSF (Exp-3) does not significantly change the simulated average temperature profiles compared with the control experiment (Exp-1). In contrast, when adding the impact of LC (Exp-4) in the surface layer (0–20 m), not only is the ME of the temperature reduced by about 0.3°C but also the MAE and root-mean-square deviation (RMSD) are improved. Adding the impact of nonbreaking waves to the model (Exp-5) reduces the ME by over 0.5°C, MAE by about 0.5°C and RMSD by about 0.65°C in the 0–20 m layer. Considering all the wave impacts (Exp-6) reduces the temperature errors much more than found in any other experiments, reducing the ME by 0.69°C, MAE by 0.56°C, and RMSD by 0.71°C in the 0–20 m layer. In the 70–100 m layer, incorporating the impact of nonbreaking waves (Exp-5) worsens the MAE and RMSD performance. Adding the various wave impacts does not improve the correlation coefficient ($R$) for the surface layer (0–20 m) in any of experiments Exp-2 to Exp-6. In this layer, the temperature change is controlled mainly by surface forcing (i.e., surface wind stress and heat flux), the wave impact significantly affecting $R$ only in the 30–110 m layer. It is in the 30–80 m layer that incorporating nonbreaking waves (Exp-5) improves $R$ the most, by increasing the mixing. In the 80–100 m layer, the impact of nonbreaking waves

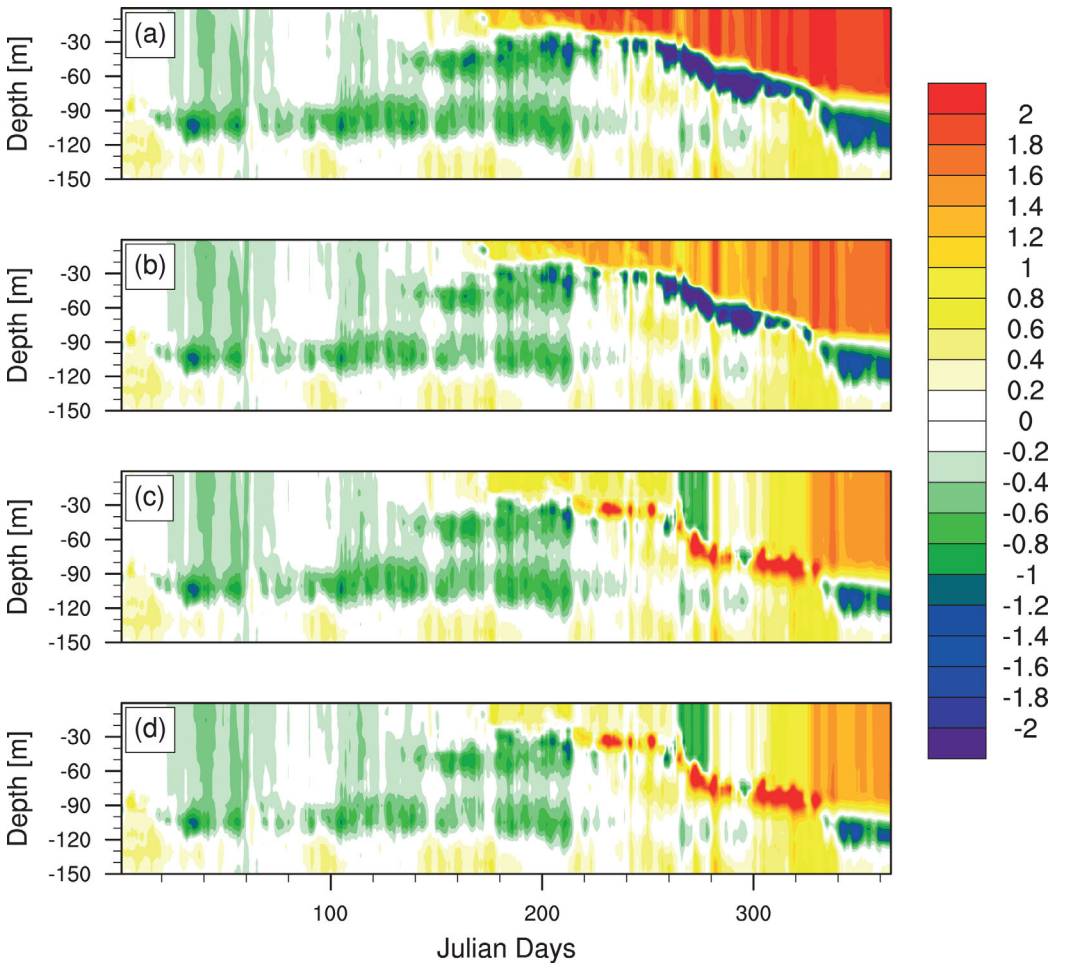


**Figure 3.** The difference between simulated results and measurements (°C) expressed as experimental minus observed results: (a) Exp-1 (no wave influence), (b) Exp-4 (only influence of LC), (c) Exp-5 (only influence of nonbreaking waves), and (d) Exp-6 (all wave influence included).

lowers *R* and increases the MAE and RMSD, possibly by overestimating the MLD. From the ME, MAE, RMSD, and R, we can see that Exp-6 performs the best of all the experiments. Comparing the various wave impact aspects indicates that nonbreaking-wave-induced mixing exerts a dominant effect, the second most important process being LC.

The TKE terms of the experiments are shown in Figure 5, the left-hand plots showing the averages for summer (June–August) and the right-hand plots the averages for winter (December–February). In summer, the TKE is mainly in the upper 40 m; in contrast, the TKE is in the upper 100 m in winter because the high winds and waves cause more TKE production in winter, deepening the MLD. The breaking waves and CSF do not significantly affect the results. The TKE increases when adding the effect of LC (Exp-4), due to the LC shear production. Considering the impact of nonbreaking waves (Exp-5) reduces the average TKE somewhat in the upper layer in both summer (Figure 5a) and winter (Figure 5b). This may be because of the feedback impact of the increasing viscosity, i.e., the temperature gradient decreases because of the increasing viscosity, which in turn reduces shear production and buoyancy production. In the 30–40 m layer, incorporating nonbreaking waves increases the TKE in summer (the nonbreaking-wave-induced mixing in summer is only in the upper layer). When all the wave impacts are added, the TKE is nearly the same as in Exp-4 in winter, which means that the change in the TKE is caused mainly by LC in winter. In summer, the average dissipation is similar in Exp-5 and Exp-6; in contrast, in winter, the dissipation in Exp-6 is similar to that in Exp-4 (see Figures 5c and 5d). For average shear production in the upper-ocean layer (i.e., 0–10 m), incorporating LC causes a significant increase, especially in winter (Figure 5f), while incorporating nonbreaking waves

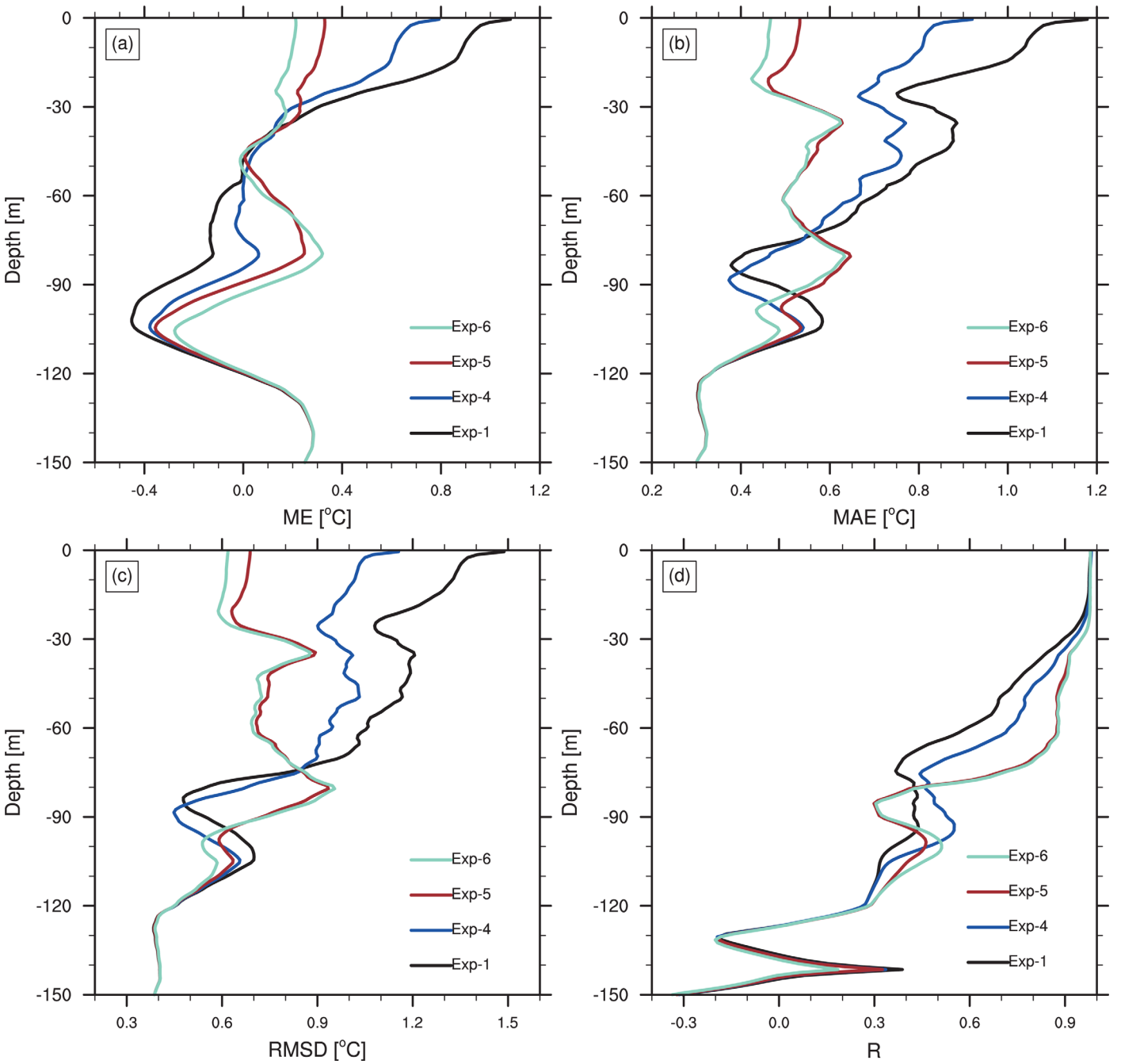


**Figure 4.** Statistical results for temperature at various depths, modeled compared with measured results: (a) mean temperature error, (b) mean absolute temperature error, (c) root-mean-square difference, and (d) correlation coefficient. No wave influence in Exp-1, only influence of LC in Exp-4, only influence of nonbreaking waves in Exp-5, and all wave influence included in Exp-6.

causes a significant reduction. In the upper-ocean layer, the increase in shear production is caused mainly by the Stokes drift. In the deep layer, in summer the total change in shear production (Exp-6) is dominated by the LC influence (Exp-4), while in winter it is dominated by nonbreaking waves (Exp-5). The feedback impact of waves on average buoyancy production is shown in Figures 5g and 5h (the change in viscosity and shear production changes the temperature gradient and, in turn, the buoyancy production). The impact of nonbreaking waves (Exp-5) mainly increases the average buoyancy production in summer and in the upper layer in winter, while the impact of LC (Exp-4) mainly increases it in winter. In the TKE terms, we can see that LC dominates the impact of waves in winter (under high-wind conditions), while the impact of non-breaking waves dominates the impact of waves in summer (under relatively low-wind conditions).

**Table 2.** Statistical Results for MLD (m) and Surface Layer (0–20 m) Temperatures (°C)

| | Exp-1 | Exp-2 | Exp-3 | Exp-4 | Exp-5 | Exp-6 |
|---|---|---|---|---|---|---|
| ME of the MLD | 16.12 | 15.98 | 15.91 | 12.07 | 5.86 | 2.99 |
| MAE of the MLD | 17.87 | 17.75 | 17.71 | 14.75 | 10.16 | 9.26 |
| ME of the temperature | 0.89 | 0.87 | 0.86 | 0.62 | 0.31 | 0.20 |
| MAE of the temperature | 1.02 | 1.01 | 1.00 | 0.80 | 0.52 | 0.46 |
| RMSD of the temperature | 1.32 | 1.30 | 1.29 | 1.02 | 0.67 | 0.61 |

The logarithmic distributions of the viscosity without and with the inclusion of nonbreaking waves are shown in Figures 6a and 6b, respectively. Compared with the low-wind conditions in summer, the turbulent mixing induced by nonbreaking waves reaches much deeper under high-wind conditions (i.e., in winter). In the surface layer, the nonbreaking-wave-induced mixing is sometimes of the same order of magnitude as that induced by other terms. Figure 7 shows the different source of TKE production: current shear production (Figure 7a), LC production (Figure 7b) and nonbreaking-wave-induced shear production (Figure 7c). Note that LC shear production decreases exponentially with depth. In the surface layer, LC shear production is larger than current shear production during most time periods. With increasing depth, current shear production dominates the shear production, exceeding LC shear production. The contribution of asymmetric-wave-motion shear to the mean flow (equation (7)) is very small (not of the same order of magnitude) compared with current shear production. Conducting the experiments with and without considering the contribution of asymmetric wave-motion to shear production (results not shown) has no significant impact on the results. It is therefore reasonable for some parameterizations [i.e., *Qiao et al*., 2004; *Hu and Wang*, 2010] of nonbreaking-wave-induced ocean mixing to exclude the contribution of nonbreaking waves to shear production.

### 4.2. Sensitivity Experiments

In some OGCMs, the Stokes drift is estimated from the wind speed. Even in some coupled systems, only the surface Stokes drift is calculated from the 2-D wave spectrum, the vertical profile being estimated using empirical formulations to reduce the computational burden. For the nonbreaking-wave-induced mixing, we use the bulk parameters for the calculation (in equations (5) and (6), the significant wave height and wave period are used to estimate $M^{SM}_{wave}$ and $l_{wave}$). Some studies use the 2-D wave spectrum to calculate the nonbreaking-wave-induced mixing parameter [e.g., *Qiao et al*., 2004]. Some authors have argued that using the 2-D wave spectrum to calculate the nonbreaking-wave-induced mixing parameter may be more appropriate [e.g., *Ghantous and Babanin*, 2014]. To determine how large an impact using the 2-D wave spectrum has on the simulation results, we choose (in this section) different parameterizations with/without the 2-D wave-spectrum information.

#### 4.2.1. Stokes Drift

The 2-D wave spectrum should be used to calculate the Stokes drift, though the wave spectrum is not always available. When the wave spectrum is unavailable, the surface Stokes drift is usually estimated from the wind speed or wind stress using formulations such as, $U_{s0}=0.016|U_{10}|$ [*Li and Garrett*, 1993] and $U_{s0}=0.377|\tau|^{1/2}$ [*Madec*, 2008], where $U_{10}$ is the wind speed at 10 m above the sea surface level. Normally, the vertical profile of the Stokes drift is calculated assuming that the surface Stokes drift exponentially decrease with depth [*Polton et al*., 2005; *Li et al*., 2013a]. *Breivik et al*. [2014] proposed a new method for estimating this vertical profile, which they demonstrate considerably improves the exponentially decreasing method [*Polton et al*., 2005; *Li et al*., 2013a], as follows:

$$\mathbf{u}_s(z)=\mathbf{u}_{s0}\frac{e^{2k_e z}}{1-8k_e z} \tag{17}$$

where $k_e$ is the inverse depth scale; for details see *Breivik et al*. [2014, 2015].

To test the impact of the 2-D wave spectrum, two more experiments were designed (Table 3). In experiment LC-1, we use the wind stress to estimate the surface Stokes drift, the vertical profile of the Stokes drift being calculated using equation (17). The direction of the Stokes drift is aligned with the wind stress. In contrast, in LC-2 we use the 2-D wave spectrum to calculate the surface Stokes drift and use equation (17) to calculate its vertical profile, as done by *Breivik et al*. [2015]. The other settings are the same as in Exp-6. From LC-1, LC-2, and Exp-6, we want to determine whether the 2-D wave spectrum is necessary for calculating the Stokes drift profile and whether it is enough to calculate only the surface Stokes drift using the 2-D wave spectrum.

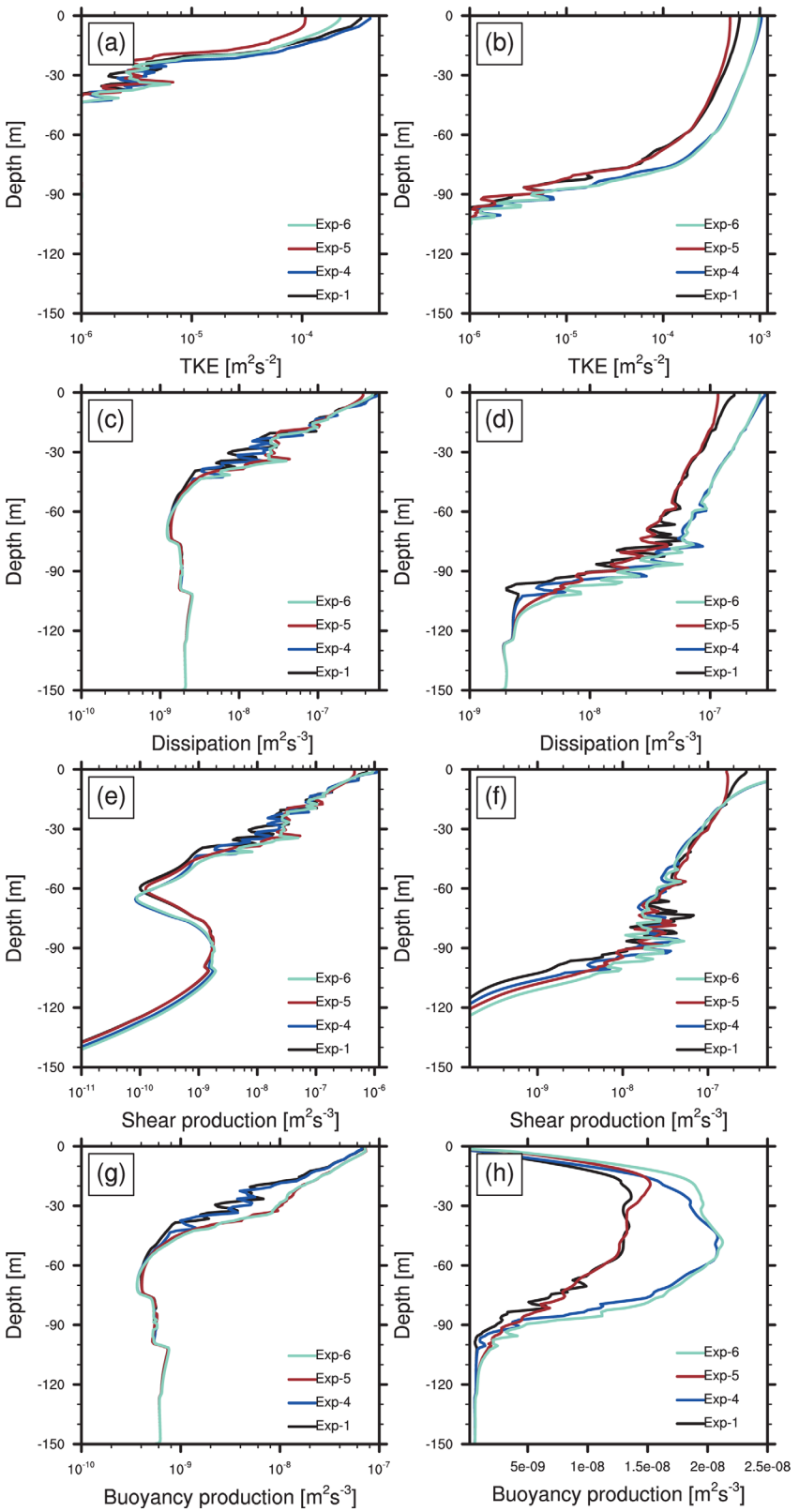


**Figure 5.** The turbulence production of different terms: average TKE in (a) summer and (b) winter; (c) average dissipation in summer and (d) winter; (e) average shear production in summer and (f) winter); and (g) average buoyancy production in summer and (h) winter. No wave influence in Exp-1, only influence of LC in Exp-4, only influence of nonbreaking waves in Exp-5, and all wave influence included in Exp-6.

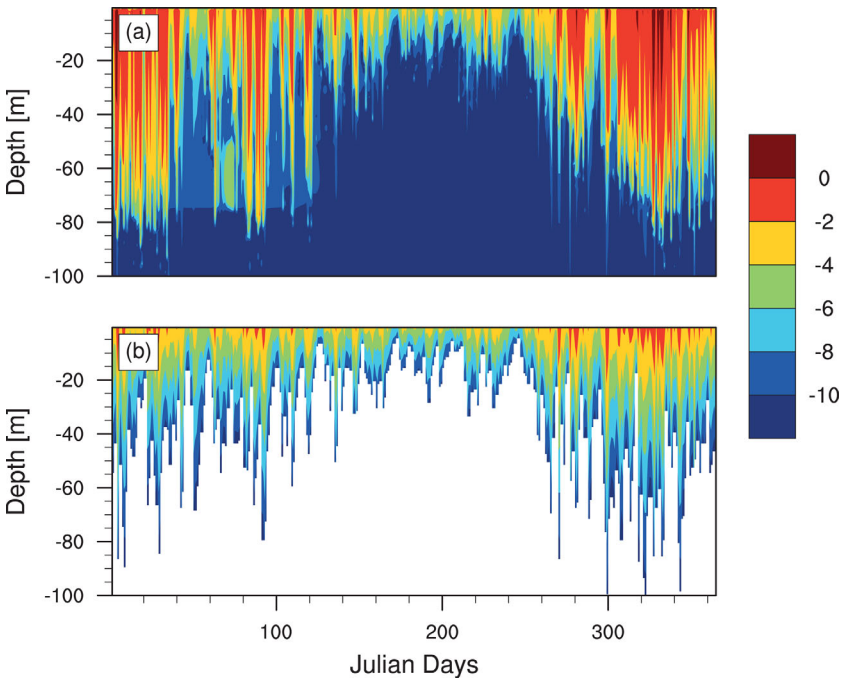


**Figure 6.** (a) Logarithmic distributions of viscosity generated by shear and (b) nonbreaking-wave-induced mixing in Exp-6; $m^2\ s^{-1}$.

The statistical results for the temperature profiles are shown in Figure 8. The ME of the temperature (Figure 8a), increases by about 0.1°C if the Stokes drift is estimated from the wind stress (LC-1). If we instead use the surface Stokes drift calculated from the 2-D wave spectrum (LC-2), this improves the results in the upper

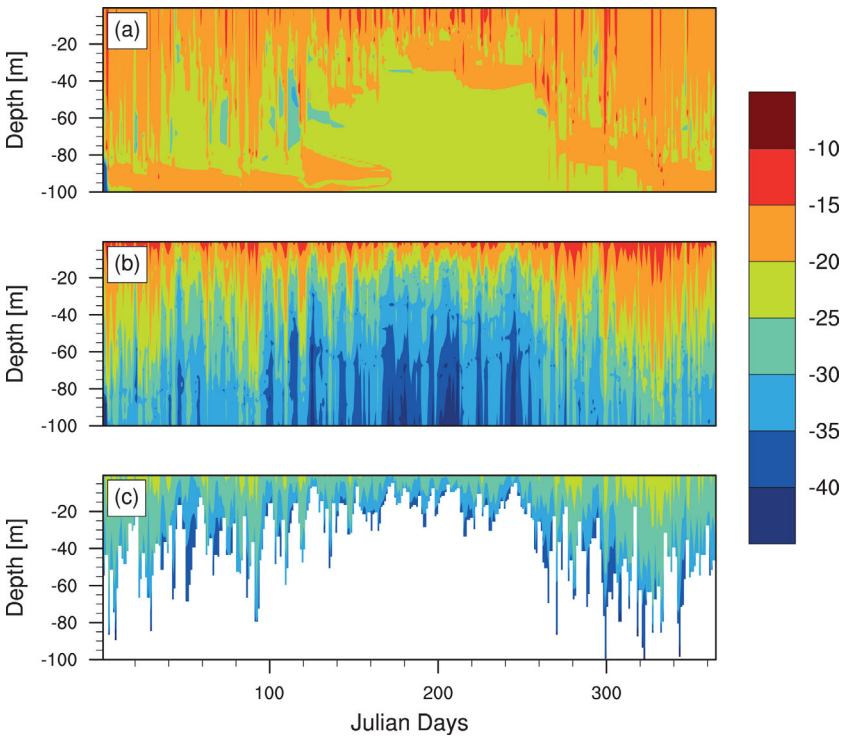


**Figure 7.** Logarithmic distributions of (a) current shear production, (b) LC production, and (c) wave production shear (equation (7)) in Exp-6; $m^2\ s^{-3}$.

**Table 3.** Sensitivity Experiments on the Stokes Drift[a]

| Experiments | Method for Calculating the Stokes Drift |
|---|---|
| Exp-6 | Surface and vertical profile of Stokes drift calculated using equation (3) |
| LC-1 | $U_{s0}$ calculated using $U_{s0}=0.377\|\tau\|^{1/2}$ and the vertical profile using equation (17) |
| LC-2 | $U_{s0}$ calculated using 2-D wave spectrum and the vertical profile using equation (17) |

[a]Exp-6 is the Reference Case and LC-1 and LC-2 investigate the importance of the 2-D wave spectrum when calculating the stokes drift.

layer insignificantly compared with LC-1. In the deep layer, the results of experiments LC-1 and LC-2 differ only slightly. Although the Stokes drift is mainly in the upper-ocean layer (the upper 40 m in this case), feedback from it influences the simulations in a much deeper layer. For the MAE of the temperature (Figure 8b), the results are similar to the ME results for the temperature. The average improvement in the MAE is more than 0.05°C in the surface layer if the Stokes drift is calculated from the 2-D wave spectrum (Exp-6) compared with LC-1 and LC-2. The differences extend to a depth of about 110 m. The RMSD results are similar to the MAE results, the coefficient in the top 30 m being almost the same in Exp-6, LC-1, and LC-2; however in the 30–110 m layer, Exp-6 performs better.

#### 4.2.2. Nonbreaking Waves

Regarding the impact of surface waves on ocean mixing, nonbreaking-wave-induced mixing is one of the most important terms (see the results in section 4.1). Here we compare three parameterizations of the impact of nonbreaking waves on ocean mixing (Table 4). Experiment Bv-1 uses the parameterization of *Qiao et al*. [2004], while experiment Bv-2 uses the parameterization of *Hu and Wang* [2010].

In parameterizing of wave-induced turbulent viscosity, *Pleskachevsky et al*. [2011] used the bulk properties (i.e., significant wave height and wave period) to calculate the nonbreaking-wave-induced mixing. In contrast to *Pleskachevsky et al*. [2011], *Qiao et al*. [2004] used the full wave spectrum to calculate the nonbreaking-wave-induced mixing parameter, as follows:

$$\nu_{wave}=\alpha\iint_{\vec{k}}E(\vec{k})e^{2kz}d\vec{k}\,\frac{\partial}{\partial z}\left[\iint_{\vec{k}}\omega^2E(\vec{k})e^{2kz}d\vec{k}\right]^{1/2} \tag{18}$$

where $\alpha$ is a coefficient (treated as 1 here), $E(\vec{k})$ the wave number spectrum, $k$ the wave number, and $\omega$ the wave angular frequency. *Hu and Wang* [2010] also used the bulk properties to calculate the nonbreaking-wave-induced mixing, expressing as

$$\nu_{wave}=\frac{2\kappa^2}{g}\delta\beta^3U_{10}^3\exp\left(\frac{gz}{\beta^2U_{10}^2}\right) \tag{19}$$

where $\kappa$ is the von Karman constant, $\delta$ the wave steepness ($\delta=2a/\lambda$, $a$ being the amplitude and $\lambda$ the wavelength), $\beta$ the wave age ($0<\beta<1$ for a growing wave and $\beta=1$ for a mature wave).

The statistical results for the temperature profiles are shown in Figure 9. In the 0–70 m layer, experiment Exp-6 performs the best, though in the 70–100 m layer, the experiment Bv-1 performs the best in terms of the ME, MAE, RMSD, and R. Experiment Bv-2 overestimates the nonbreaking-wave-induced mixing in the ocean. Figure 10 shows the temperature differences between the simulation results and the measurements. Note that Exp-6 overestimates the MLD, so it performs poorly in the 70–100 m layer; in contrast, experiment Bv-1 still underestimates the MLD.

## 5. Discussion

Comparing the different impacts of surface waves (i.e., breaking waves, CSF, LC, nonbreaking waves) indicates that nonbreaking waves play the most important role in ocean mixing, LC being the second most important wave term. Considering the combined impact of all the wave types results in the best performance (Exp-6). Here we use a $k-\epsilon$ model, but the results are similar when applying the same wave impacts in a higher-order closure scheme, i.e., the MY model (results not shown). LC increases the total shear production and the TKE (see Figure 5), in turn increasing the viscosity in the upper-ocean surface layer. Because

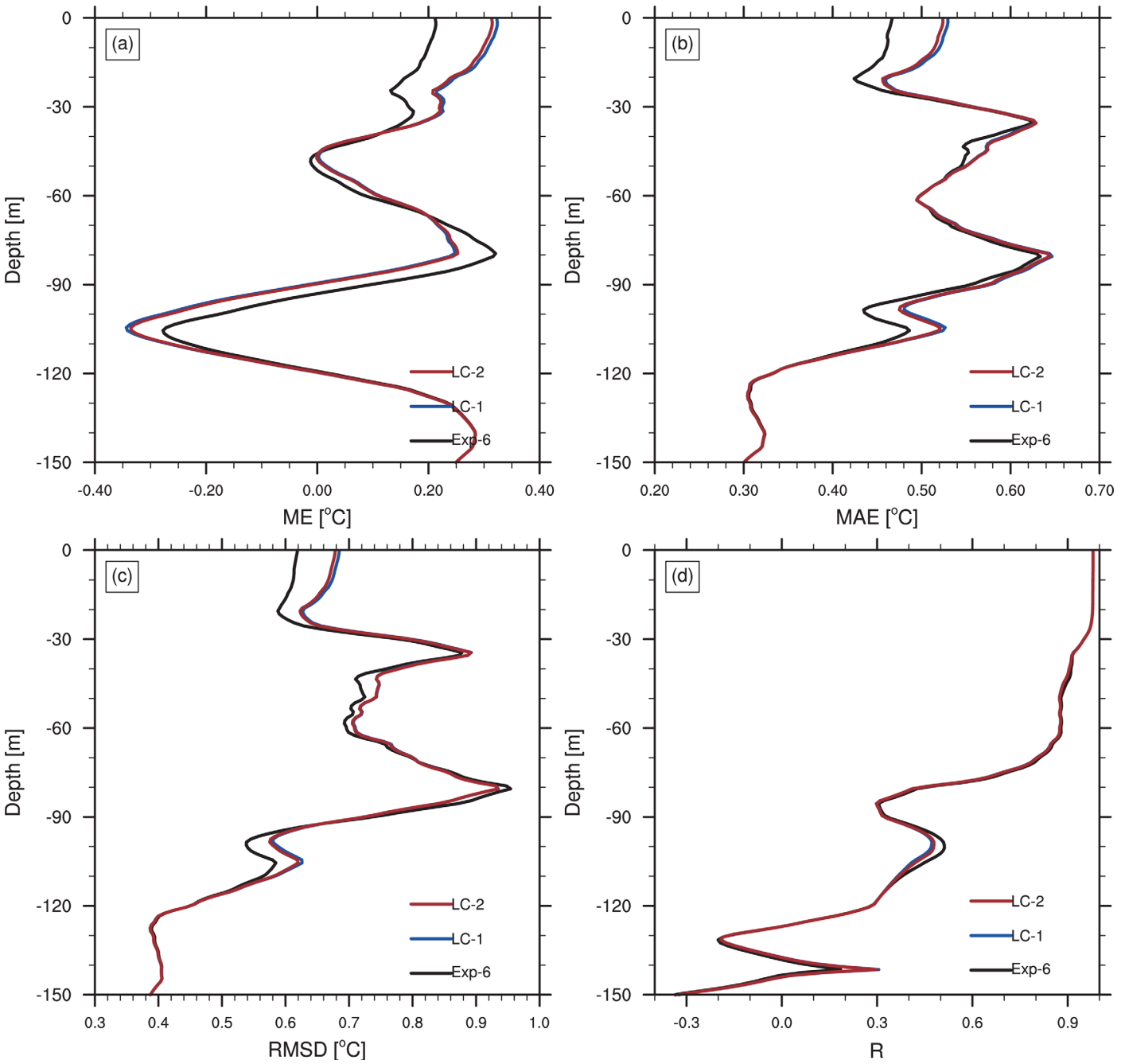


**Figure 8.** As in Figure 4 except for Exp-6, LC-1, and LC-2.

the Stokes drift decreases exponentially with depth, the shear produced by LC decreases with depth, meaning that the direct impact of LC is mainly on the upper-ocean layer. The change of shear production will change the temperature gradients and buoyancy production. Although the direct influence of the shear

**Table 4.** Sensitivity Experiments on Nonbreaking Wave Impact[a]

| Experiments | Parameterizations of the Impact of Nonbreaking Waves |
|---|---|
| Exp-6 | Parameterization from *Pleskachevsky et al.* [2011] |
| Bv-1 | Parameterization from *Qiao et al.* [2004] |
| Bv-2 | Parameterization from *Hu and Wang* [2010] |

[a]Exp-6 is the Reference Case, and Bv-1 and Bv-2 are parameterizations of the impact of nonbreaking waves.

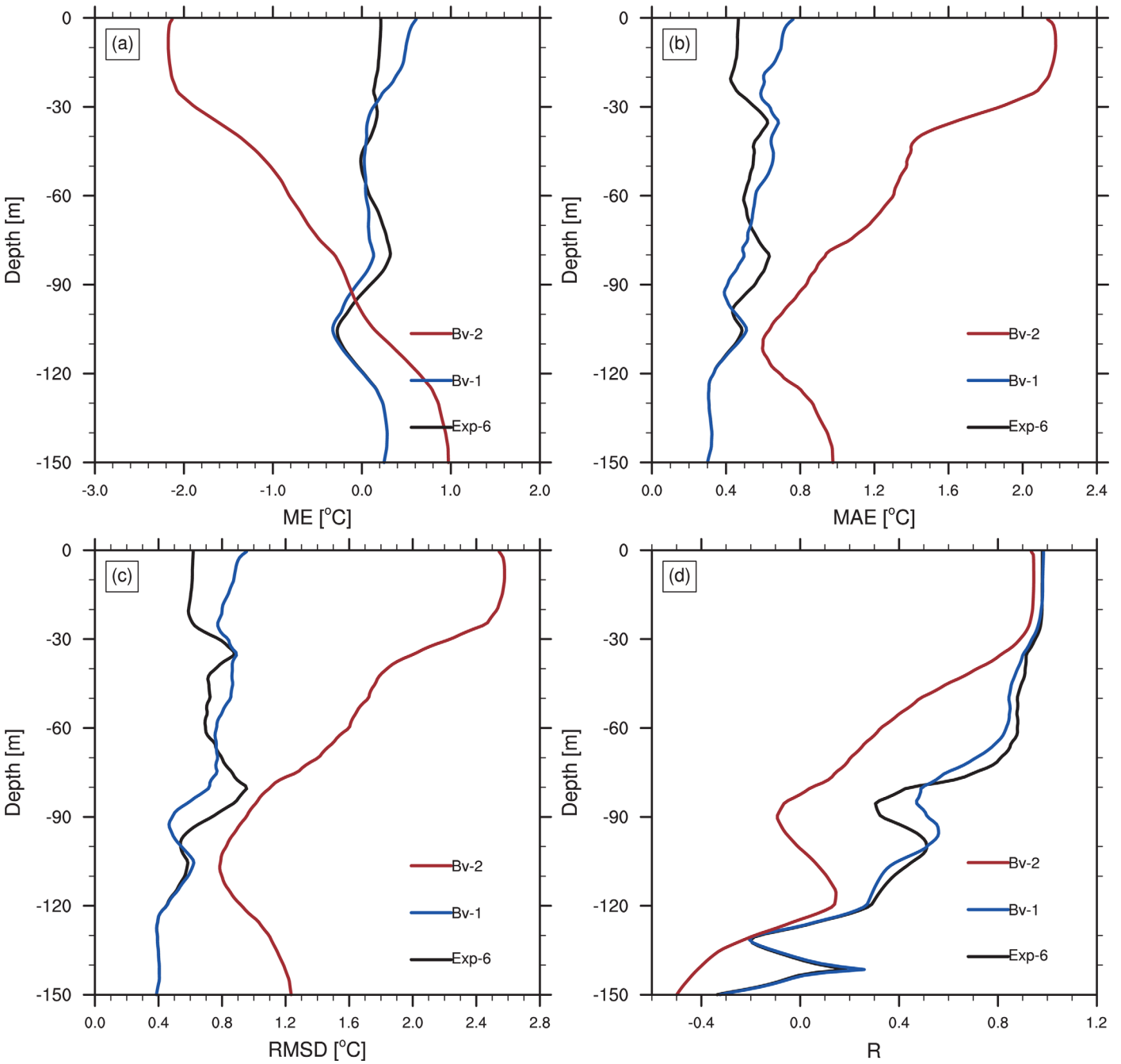


**Figure 9.** As in Figure 4 except for Exp-6, Bv-1, and Bv-2.

production by LC is mainly on the upper layer, the change of the temperature gradients will impact on more deeper layer (see Figure 4). Nonbreaking waves influence upper-ocean mixing in two ways: through the nonbreaking-wave-induced mixing, and through the contribution of nonbreaking waves to total shear production. The nonbreaking wave contribution to shear production is very small, the main impact being from nonbreaking-wave-induced mixing. Taking account of nonbreaking-wave-induced mixing reduces the total shear production compared with experiments ignoring the impact of nonbreaking waves in the upper-ocean layer. However, considering this mixing increase the total shear production in the deep layer (see Figures 5e and 5f), possible due to feedback from the increased viscosity in the model.

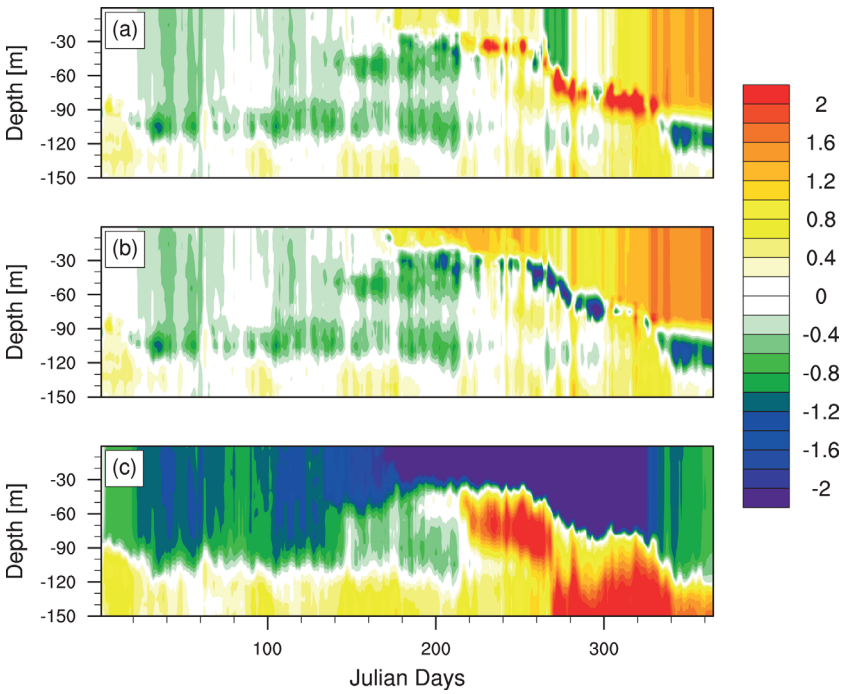


**Figure 10.** As in Figure 3 except for (a) Exp-6, (b) Bv-1, and (c) Bv-2.

In some simulation periods, the model overestimates the MLD of ocean mixing when inducing the impact of nonbreaking waves. One possible explanation is that the parametrization used here overestimates the nonbreaking-wave-induced mixing because the parametrization is calculated from bulk properties (i.e., significant wave height and wave period), not from the full wave spectrum. As argued by *Ghantous and Babanin* [2014], using bulk properties will deal with one value for a certain bulk properties, even the wave spectrum is different. The other possible explanation is that the horizontal advection is not considered in the model. *Li et al*. [2013b] added horizontal advection adjustment to make the model match the observations. In the present study, we focus on the relative impacts of different wave effects on ocean mixing, so advection adjustment was not introduced. As well, some artifacts may be introduced when adding the horizontal advection, which may cause some unwanted results. Although some tuning parameters (i.e., the critical Reynolds number and the ratio of breaking stress to wind stress,) which are not clear in the model, the impacts of surface waves are obvious in the results.

Estimating the Stokes drift from the wind speed is normal in uncoupled models [e.g., *Madec*, 2008]. Even ocean models coupled with wave models use only the surface Stokes drift calculated from the wave spectrum, the vertical profile being estimated from parameterizations [e.g., *Breivik et al*., 2015]. The present results indicate that the model results would be improved significantly if the vertical profile of the Stokes drift were calculated from the 2-D wave spectrum. The Stokes drift direction is usually treated as aligned with the wind direction or the same as the surface Stokes drift when the vertical profile of the Stokes drift is not calculated from the 2-D wave spectrum. In reality, the Stokes drift direction may differ from the wind direction because of the swell and the distribution of the wave spectrum. This would significantly influence the simulation results. In coupled models, the vertical profile of the Stokes drift calculated from the 2-D wave spectrum should be used to improve the model performance, if possible.

Using the nonbreaking-wave-induced ocean mixing calculated from the 2-D wave spectrum [*Qiao et al*., 2004] improves the simulation results for the upper-ocean layer, though it still underestimates the MLD and overestimates the upper-ocean-layer temperature. In contrast, using the nonbreaking-wave-induced mixing calculated from bulk properties [*Pleskachevsky et al*., 2011] overestimates the MLD. One possible reason for these results is that, in this study, the 2-D wave spectrum is simulated using WAM, which may be not very accurate. In contrast, the parameterization of *Pleskachevsky et al*. [2011] produces the same nonbreaking-

wave-induced mixing when the bulk properties are the same, even though the 2-D wave spectrum is different; this may lead to overestimation of the MLD.

The SST plays a vital role in the air-sea interaction processes, as it largely controls sensible and latent heat fluxes. Those air-sea interaction processes will then influence the dynamic circulation of the ocean and atmosphere. For tropical cyclone forecasts, the SST is also a very important term as it controls the energy transport between the ocean and atmosphere. It can influence the intensity as well as the track of tropical cyclones [*Li et al*., 2014]. Taking wave impacts on upper-ocean mixing into account to improve SST simulation is necessary, not only in climate models but also in weather forecast models.

## 6. Summary and Conclusions

Measurements made in the field and laboratory indicate that surface waves play an important role in upper-ocean mixing. Surface waves affect upper-ocean mixing mainly through four processes: wave breaking, CSF, LC, and stirring by nonbreaking waves. In this study, these four processes affecting upper-ocean mixing are introduced into the $k-\epsilon$ model within GOTM, a 1-D ocean model. The simulation of data from the Papa ocean weather station is used to investigate the impact of waves on the ocean.

Adding the impact of surface waves on the ocean mixing to the model improves its performance. As expected, adding all the wave impacts in combination results in the best model performance, while considering only the impact of breaking waves or of the CSF insignificantly affects the simulation results. Nonbreaking-wave-induced mixing and LC are the most important terms contributing to the improved model results.

The contribution of nonbreaking waves to shear production is much smaller than the contribution of the other terms. Under low-wind conditions, the average impact of nonbreaking waves on the TKE terms is more important than that of LC. In contrast, under high-wind conditions, the impact of LC is more important than that of nonbreaking waves.

In most coupled models, only the surface Stokes drift calculated from the 2-D wave spectrum is used. The present results indicate that using the 2-D wave spectrum to calculate the Stokes drift vertical profile is more accurate and can improve the model results. In further model development, we suggest using the 2-D wave spectrum to calculate the vertical profile of the Stokes drift if possible.

The nonbreaking-wave-induced mixing calculated from bulk parameters chosen here overestimates the MLD. However, the parameterization that *Qiao et al*. [2004] calculated from the full wave spectrum still underestimates the MLD; the various potential reasons for this merit further study.

Although this study entails some uncertainties because of its tuning parameters and because of the limitations of the 1-D ocean model, it clearly demonstrates that surface waves have a considerable impact on upper-ocean mixing. In further coupled model development, it is necessary to consider the wave information used in ocean models, and 2-D wave spectrum information should be used to calculate the vertical profile of the Stokes drift.

**Acknowledgments**
Lichuan Wu is supported by the Swedish Research Council (project 2012–3902). The OCS Project Office of NOAA/PMEL is acknowledged for providing access to the measurements at Papa station. The insightful comments from two anonymous reviewers helped improving the manuscript. The data in the figures and tables can be acquired by contacting the first author.

## References

Ardhuin, F., and A. D. Jenkins (2006), On the interaction of surface waves and upper ocean turbulence, *J. Phys. Oceanogr.*, *36*(3), 551–557.
Axell, L. B. (2002), Wind-driven internal waves and Langmuir circulations in a numerical ocean model of the southern Baltic sea, *J. Geophys. Res.*, *107*(C11), 3204, doi:10.1029/2001JC000922.
Babanin, A. (2006), On a wave-induced turbulence and a wave-mixed upper ocean layer, *Geophys. Res. Lett.*, *33*, L20605, doi:10.1029/2006GL027308.
Babanin, A. V., and D. Chalikov (2012), Numerical investigation of turbulence generation in non-breaking potential waves, *J. Geophys. Res.*, *117*, C06010, doi:10.1029/2012JC007929.
Belcher, S. E., et al. (2012), A global perspective on Langmuir turbulence in the ocean surface boundary layer, *Geophys. Res. Lett.*, *39*, L18605, doi:10.1029/2012GL052932.
Breivik, Ø., P. A. Janssen, and J.-R. Bidlot (2014), Approximate stokes drift profiles in deep water, *J. Phys. Oceanogr.*, *44*(9), 2433–2445.
Breivik, Ø., K. Mogensen, J.-R. Bidlot, M. A. Balmaseda, and P. A. Janssen (2015), Surface wave effects in the Nemo ocean model: Forced and coupled experiments, *J. Geophys. Res. Oceans*, *120*, 2973–2992, doi:10.1002/2014JC010565.
Burchard, H., K. Bolding, and M. Villarreal (1999), GOTM, a general oceanturbulence model: Theory, implementation and test cases, Rep. EUR18745, 103 pp., Eur. Comm.
Craig, P. D., and M. L. Banner (1994), Modeling wave-enhanced turbulence in the ocean surface layer, *J. Phys. Oceanogr.*, *24*(12), 2546–2559.
Craik, A. D., and S. Leibovich (1976), A rational model for Langmuir circulations, *J. Fluid Mech.*, *73*(03), 401–426.

Dai, D., F. Qiao, W. Sulisz, L. Han, and A. Babanin (2010), An experiment on the nonbreaking surface-wave-induced vertical mixing, *J. Phys. Oceanogr.*, *40*(9), 2180–2188.
D'Asaro, E. A. (2014), Turbulence in the upper-ocean mixed layer, *Annu. Rev. Mar. Sci.*, *6*, 101–115.
Deng, Z., L. Xie, G. Han, X. Zhang, and K. Wu (2012), The effect of Coriolis-Stokes forcing on upper ocean circulation in a two-way coupled wave-current model, *Chin. J. Oceanol. Limnol.*, *30*, 321–335.
Deng, Z., L. Xie, T. Yu, S. Shi, J. Jin, and K. Wu (2013), Numerical study of the effects of wave-induced forcing on dynamics in ocean mixed layer, *Adv. Meteorol.*, Article ID: 365818, 10 pp., doi:10.1155/2013/365818.
Drivdal, M., G. Broström, and K. Christensen (2014), Wave-induced mixing and transport of buoyant particles: Application to the statfjord a oil spill, *Ocean Sci.*, *10*(6), 977–991.
Fan, Y., and S. M. Griffies (2014), Impacts of parameterized Langmuir turbulence and nonbreaking wave mixing in global climate simulations, *J. Clim.*, *27*(12), 4752–4775.
Ghantous, M., and A. Babanin (2014), One-dimensional modelling of upper ocean mixing by turbulence due to wave orbital motion, *Nonlinear Processes Geophys.*, *21*(1), 325–338.
Grant, A. L., and S. E. Belcher (2009), Characteristics of Langmuir turbulence in the ocean mixed layer, *J. Phys. Oceanogr.*, *39*(8), 1871–1887.
He, H., and D. Chen (2011), Effects of surface wave breaking on the oceanic boundary layer, *Geophys. Res. Lett.*, *38*, L07604, doi:10.1029/2011GL046665.
Hu, H., and J. Wang (2010), Modeling effects of tidal and wave mixing on circulation and thermohaline structures in the Bering sea: Process studies, *J. Geophys. Res.*, *115*, C01006, doi:10.1029/2008JC005175.
Huang, C. J., and F. Qiao (2010), Wave-turbulence interaction and its induced mixing in the upper ocean, *J. Geophys. Res.*, *115*, C04026, doi:10.1029/2009JC005853.
Huang, C. J., F. Qiao, Z. Song, and T. Ezer (2011), Improving simulations of the upper ocean by inclusion of surface waves in the Mellor-Yamada turbulence scheme, *J. Geophys. Res.*, *116*, C01007, doi:10.1029/2010JC006320.
Janssen, P. A. (2012), Ocean wave effects on the daily cycle in SST, *J. Geophys. Res.*, *117*, C00J32, doi:10.1029/2012JC007943.
Kantha, L. H., and C. A. Clayson (2004), On the effect of surface gravity waves on mixing in the oceanic mixed layer, *Ocean Modell.*, *6*(2), 101–124.
Kantha, L., H. Tamura, and Y. Miyazawa (2014), Comment on wave-turbulence interaction and its induced mixing in the upper ocean by Huang and Qiao, *J. Geophys. Res. Oceans*, *119*, 1510–1515, doi:10.1002/2013JC009318.
Langmuir, I., et al. (1938), Surface motion of water induced by wind, *Science*, *87*(2250), 119–123.
Li, M., and C. Garrett (1993), Cell merging and the jet/downwelling ratio in Langmuir circulation, *J. Mar. Res.*, *51*(4), 737–769.
Li, M., K. Zahariev, and C. Garrett (1995), Role of Langmuir circulation in the deepening of the ocean surface mixed layer, *Science*, *270*(5244), 1955–1957.
Li, M., C. Garrett, and E. Skyllingstad (2005), A regime diagram for classifying turbulent large eddies in the upper ocean, *Deep Sea Res., Part I*, *52*(2), 259–278.
Li, S., J. Song, and W. Fan (2013a), Effect of Langmuir circulation on upper ocean mixing in the south china sea, *Acta Oceanol. Sin.*, *32*(3), 28–33.
Li, Y., F. Qiao, X. Yin, Q. Shu, and H. Ma (2013b), The improvement of the one-dimensional Mellor-Yamada and k-profile parameterization turbulence schemes with the non-breaking surface wave-induced vertical mixing, *Acta Oceanol. Sin.*, *32*(9), 62–73.
Li, Y., S. Peng, J. Wang, and J. Yan (2014), Impacts of nonbreaking wave-stirring-induced mixing on the upper ocean thermal structure and typhoon intensity in the south Cshina sea, *J. Geophys. Res. Oceans*, *119*, 5052–5070, doi:10.1002/2014JC009956.
Madec, G. (2008), Nemo ocean engine, *Note du Pôle de modélisation*, Inst. Pierre-Simon Laplace, France.
McWilliams, J. C., and P. P. Sullivan (2000), Vertical mixing by Langmuir circulations, *Spill Sci. Technol. Bull.*, *6*(3), 225–237.
McWilliams, J. C., P. P. Sullivan, and C.-H. Moeng (1997), Langmuir turbulence in the ocean, *J. Fluid Mech.*, *334*, 1–30.
Mellor, G., and A. Blumberg (2004), Wave breaking and ocean surface layer thermal response, *J. Phys. Oceanogr.*, *34*(3), 693–698.
Mellor, G. L., and T. Yamada (1982), Development of a turbulence closure model for geophysical fluid problems, *Rev. Geophys.*, *20*(4), 851–875.
Melville, W. K., F. Veron, and C. J. White (2002), The velocity field under breaking waves: Coherent structures and turbulence, *J. Fluid Mech.*, *454*, 203–233.
Noh, Y., H. S. Min, and S. Raasch (2004), Large eddy simulation of the ocean mixed layer: The effects of wave breaking and Langmuir circulation, *J. Phys. Oceanogr.*, *34*(4), 720–735.
Paskyabi, M. B., and I. Fer (2014), Turbulence structure in the upper ocean: A comparative study of observations and modeling, *Ocean Dyn.*, *64*(4), 611–631.
Paskyabi, M. B., I. Fer, and A. D. Jenkins (2012), Surface gravity wave effects on the upper ocean boundary layer: Modification of a one-dimensional vertical mixing model, *Cont. Shelf Res.*, *38*, 63–78.
Pleskachevsky, A., M. Dobrynin, A. V. Babanin, H. Günther, and E. Stanev (2011), Turbulent mixing due to surface waves indicated by remote sensing of suspended particulate matter and its implementation into coupled modeling of waves, turbulence, and circulation, *J. Phys. Oceanogr.*, *41*(4), 708–724.
Polton, J. A., D. M. Lewis, and S. E. Belcher (2005), The role of wave-induced Coriolis-Stokes forcing on the wind-driven mixed layer, *J. Phys. Oceanogr.*, *35*(4), 444–457.
Qiao, F., and C. J. Huang (2012), Comparison between vertical shear mixing and surface wave-induced mixing in the extratropical ocean, *J. Geophys. Res.*, *117*, C00J16, doi:10.1029/2012JC007930.
Qiao, F., Y. Yuan, Y. Yang, Q. Zheng, C. Xia, and J. Ma (2004), Wave-induced mixing in the upper ocean: Distribution and application to a global ocean circulation model, *Geophys. Res. Lett.*, *31*, L11303, doi:10.1029/2004GL019824.
Qiao, F., Y. Yuan, T. Ezer, C. Xia, Y. Yang, X. Lü, and Z. Song (2010), A three-dimensional surface wave-ocean circulation coupled model and its initial testing, *Ocean Dyn.*, *60*(5), 1339–1355.
Qiao, F., Z. Song, Y. Bao, Y. Song, Q. Shu, C. Huang, and W. Zhao (2013), Development and evaluation of an earth system model with surface gravity waves, *J. Geophys. Res. Oceans*, *118*, 4514–4524, doi:10.1002/jgrc.20327.
Savelyev, I. B., E. Maxeiner, and D. Chalikov (2012), Turbulence production by nonbreaking waves: Laboratory and numerical simulations, *J. Geophys. Res.*, *117*, C00J13, doi:10.1029/2012JC007928.
Smyth, W. D., E. D. Skyllingstad, G. B. Crawford, and H. Wijesekera (2002), Nonlocal fluxes and stokes drift effects in the k-profile parameterization, *Ocean Dyn.*, *52*(3), 104–115.
Sullivan, P. P., J. C. McWilliams, and W. K. Melville (2004), The oceanic boundary layer driven by wave breaking with stochastic variability. Part 1: Direct numerical simulations, *J. Fluid Mech.*, *507*, 143–174.

Sullivan, P. P., J. C. McWilliams, and W. K. Melville (2007), Surface gravity wave effects in the oceanic boundary layer: Large-eddy simulation with vortex force and stochastic breakers, *J. Fluid Mech.*, *593*, 405–452.
Sutherland, G., B. Ward, and K. Christensen (2013), Wave-turbulence scaling in the ocean mixed layer, *Ocean Sci.*, *9*(4), 597–608.
Terray, E., M. Donelan, Y. Agrawal, W. Drennan, K. Kahma, A. Williams, P. Hwang, and S. Kitaigorodskii (1996), Estimates of kinetic energy dissipation under breaking waves, *J. Phys. Oceanogr.*, *26*(5), 792–807.
Tsai, W.-t., S.-m. Chen, and G.-h. Lu (2015), Numerical evidence of turbulence generated by nonbreaking surface waves, *J. Phys. Oceanogr.*, *45*(1), 174–180.
Umlauf, L., and H. Burchard (2005), Second-order turbulence closure models for geophysical boundary layers. a review of recent work, *Cont. Shelf Res.*, *25*(7), 795–827.
Uppala, S. M., et al. (2005), The ERA-40 re-analysis, *Q. J. R. Meteorol. Soc.*, *131*(612), 2961–3012.
WAMDI (1988), The WAM model: A third generation ocean wave prediction model, *J. Phys. Oceanogr.*, *18*(12), 1775–1810.
Weller, R., A. Fischer, D. Rudnick, C. Eriksen, T. Dickey, J. Marra, C. Fox, and R. Leben (2002), Moored observations of upper-ocean response to the monsoons in the Arabian sea during 1994–1995, *Deep Sea Res., Part II*, *49*(12), 2195–2230.
Wu, K., and B. Liu (2008), Stokes drift-induced and direct wind energy inputs into the Ekman layer within the Antarctic circumpolar current, *J. Geophys. Res.*, *113*, C10002, doi:10.1029/2007JC004579.